Structure-function relationships underpin disulfide loop cleavage-dependent activation of *Legionella pneumophila* lysophosholipase A PlaA

Miriam Hiller1#, Maurice Diwo2#, Sabrina Wamp1, Thomas Gutsmann3, Christina Lang1, Wulf Blankenfeldt2,4*, Antje Flieger1*

1 Division of Enteropathogenic Bacteria and Legionella (FG11), Robert Koch Institute, Burgstr. 37, 38855 Wernigerode, Germany.

2 Structure and Function of Proteins, Helmholtz Centre for Infection Research, Inhoffenstrasse 7, 38124 Braunschweig, Germany.

3 Research Center Borstel, Leibniz Lung Center, Division of Biophysics, Parkallee 10, 23845 Borstel, Germany; CSSB – Centre for Structural Systems Biology, Hamburg, Germany

4 Institute for Biochemistry, Biotechnology and Bioinformatics, Technische Universität Braunschweig, Braunschweig, Germany.

* corresponding authors: Antje Flieger and Wulf Blankenfeldt

Email: fliegera@rki.de and wulf.blankenfeldt@helmholtz-hzi.de;

# and * contributed equally

ORCID Antje Flieger 0000-0003-3819-2979, Sabrina Wamp 0000-0002-0387-4171,

Wulf Blankenfeldt: 0000-0001-9886-9668, Thomas Gutsmann: 0000-0001-5061-7891

Running title:

Activation of *Legionella pneumophila* lysophosholipase A PlaA

Keywords:

Legionella, phospholipase, GDSL enzyme, activation, 3D structure, disulphide loop, zinc metalloprotease

Abstract

Legionella pneumophila, the causative agent of a life-threatening pneumonia, intracellularly replicates in a specialized compartment in lung macrophages, the *Legionella*-containing vacuole (LCV). Secreted proteins of the pathogen govern important steps in the intracellular life cycle including bacterial egress. Among these is the type II secreted PlaA which, together with PlaC and PlaD, belongs to the GDSL phospholipase family found in *L. pneumophila*. PlaA shows lysophospholipase A (LPLA) activity which increases after secretion and subsequent processing by the zinc metalloproteinase ProA at residue E266/L267 located within a disulfide loop. Activity of PlaA contributes to the destabilization of the LCV in the absence of the type IVB-secreted effector SdhA. We here present the 3D structure of PlaA which shows a typical α/β hydrolase fold and reveals that the uncleaved disulfide loop forms a lid structure covering the catalytic triad S30/D278/H282. This leads to reduction of both substrate access and membrane interaction before activation; however, the catalytic and membrane interaction site gets more accessible when the disulfide loop is processed. After structural modelling, a similar activation process is suggested for the GDSL hydrolase PlaC, but not for PlaD. Furthermore, the size of the PlaA substrate binding site indicated preference towards phospholipids comprising ~16 carbon fatty acid residues which was verified by lipid hydrolysis, suggesting a molecular ruler mechanism. Indeed, mutational analysis changed the substrate profile with respect to fatty acid chain length. In conclusion, our analysis revealed the structural basis for the regulated activation and substrate preference of PlaA.

53 **Introduction**

54

55 *Legionella pneumophila* is ubiquitously found in aqueous habitats, multiplies within environmental
56 amoebae, and is an important bacterial lung pathogen (1,2). From its natural habitat, *L. pneumophila* is
57 transmitted via aerosols into the human lung where lung macrophages serve as the primary replication
58 site. The infection process in mammalian cells and in amoeba shows many similarities. In both, the
59 bacteria apply means to withstand the multifaceted host defenses and subsequently replicate within a
60 specialized phagosome, termed the *Legionella*-containing vacuole (LCV) (3). Establishment of an intact
61 replication vacuole and its maintenance - for the time of bacterial replication - is essential for *Legionella*
62 propagation and requires a variety of bacterial and host factors (4,5). Several bacterial gene loci
63 contribute to intracellular establishment and replication of *L. pneumophila* and here secretion systems,
64 especially the type IVB (T4BSS) Dot/Icm and the type II (T2SS) Lsp systems, and their transported
65 effectors are major determinants (6-10). It has been shown that phospholipases are among the secreted
66 effectors and affect establishment and maintenance of the LCV. For example, patatin-like phospholipases
67 VipD and VpdC, both exported via the type IVB Dot/Icm machinery, influence lipid composition of
68 endosomes fusing to the LCV or vacuolar expansion by regulating lysophospholipid content, respectively
69 (11-14). Further, phospholipases are required to exit the LCV and the host after completed replication
70 and their involvement has been shown for a variety of pathogens including *L. pneumophila* (15-17).

71

72 Phospholipases are important virulence factors of pathogens (18) and classify into four major functional
73 groups based on the position at which they cleave within a phospholipid, specifically phospholipases A
74 (PLA), phospholipases B (PLB), phospholipases C (PLC), and phospholipases D (PLD). PLAs, like VipD or
75 VpdC, hydrolyze the carboxylester bonds at sn-1 or sn-2 position and thereby release fatty acids. If only
76 one fatty acid is targeted, a lysophospholipid is generated and may be further cleaved by a
77 lysophospholipase A (LPLA), liberating the remaining fatty acid. At least 19 phospholipases are found in
78 *L. pneumophila*, comprising 15 PLAs, three PLCs, and one PLD. The PLAs are divided into the patatin-like
79 phospholipases (incl. VipD and VpdC), the PlaB-like, and the GDSL enzymes (19-21).

80

81 *L. pneumophila* possesses three GDSL enzymes PlaA, PlaC, and PlaD, on which this study is focused (Fig.
82 1A). The family of GDSL hydrolases is characterized by five conserved amino acid sequence blocks
83 (19,22,23). The first block is located near the N-terminus and contains the active site serine embedded in
84 a Gly-Asp-Ser-Leu (GDSL) motif as opposed to the Gly-X-Ser-X-Gly motif commonly found in other lipases.
85 The catalytic triad of GDSL hydrolases is completed by aspartate and histidine located in the fifth

86 conserved block. GDSL hydrolases have a flexible active site that allows for broad substrate specificity
87 and enzyme activities range from protease to arylesterase to PLA/LPLA and
88 glycerophospholipid:cholesterol acyltransferase (GCAT) activities. The latter transfers phospholipid-
89 bound fatty acids to the acceptor molecule cholesterol (22,23).
90
91 The three enzymes differ with regard to activities, molecular weight, and mode of secretion (Tab. 1, Fig.
92 1A). PlaA mainly shows LPLA and GCAT activities while PlaC reveals PLA and GCAT activities (24-26). PlaA
93 and PlaC, which have molecular weights of 34.4 and 49.7 kDa, respectively, harbor a predicted sec signal
94 peptide (SP) and are both secreted via the T2SS Lsp. Interestingly, the proteins observed in culture
95 supernatants were considerably smaller after reducing SDS-PAGE, specifically ~25-28 kDa and ~36 kDa,
96 respectively (26,27). This was however not the case for culture supernatants of a *L. pneumophila* knock
97 out mutant in the type II-secreted zinc metalloproteinase ProA which suggested processing of PlaA and
98 PlaC by ProA (26,27). The respective preferred cleavage sites of ProA were analyzed and are located
99 within disulfide loop structures of both proteins. For PlaA, the preferred site was determined as
100 E266/L267. Cleavage of the disulfide loop by ProA or disulfide loop truncation by mutagenesis is
101 associated with an increase in enzymatic activity of PlaA and PlaC (26,27). Specifically, PlaA LPLA but not
102 GCAT activity and PlaC PLA and GCAT activities are activated by ProA (26,27). However, the mechanism is
103 not understood from a structure-centered view. The 59.6 kDa protein PlaD has not been characterized
104 extensively, lacks a predicted sec secretion signal, and it is not secreted into the culture supernatant
105 upon growth in broth medium (27).
106
107 Relevance of PlaA and PlaC during host cell infection was shown for both enzymes. Specifically, in the
108 absence of the T4BSS effector SdhA, which is important for LCV stabilization, PlaA can disrupt the
109 vacuole membrane such that the bacteria get access to the cytosol, i.e. prematurely egress from the LCV
110 and, as a consequence, host cell death pathways are triggered (15,28). Further, a *L. pneumophila* GDSL
111 triple mutant showed reduced cell exit (17). Therefore, PlaA may be an important factor supporting
112 bacterial LCV and host egress after intracellular replication. In line with these functions, PlaA and its
113 activity is detected from mid-exponential growth phase on and is most prominent in late-logarithmic
114 growth phase (29,30). Also, PlaC is more abundant during stationary phase than during logarithmic
115 growth phase and shows a functional overlap with the aminopeptidase LapA (30,31). Although *plaC* and
116 *lapA* individually seemed dispensable for host infections, *L. pneumophila plaC/lapA* double mutants
117 show a severe replication defect in host amoebae (31).
118

119 Since many of the pathogen phospholipases are capable to attack cellular membranes, such enzymes
120 may also damage the pathogen itself before export. Therefore, sophisticated activation mechanisms
121 might be required for example to prevent self-inflicted damage to the producer or to spacially regulate
122 activity. Such mechanisms are multifaceted and include the following: 1) oligomerization as found in *E.*
123 *coli* PldA (32), 2) deoligomerization as described for *L. pneumophila* PlaB or *P. aeruginosa* PlaF (21,33,34),
124 interaction with accessory factors, such as 3) metal ions described for *L. pneumophila* PLCs (35), 4)
125 chemical modification, such as ubiquitination of VpdC (14), or 5) host or bacterial protein cofactors, as
126 Rab5/Rab22 found for *L. pneumophila* VipD (11-13), and 6) proteolytic processing of proenzymes. As
127 outlined above, the latter proteolysis-based activation is described for *L. pneumophila* PlaA and PlaC
128 (26,27,36).
129
130 We present here the crystal structure of PlaA as basis for the clarification of structure-function
131 relationships in disulfide loop cleavage-dependent enzyme activation. The PlaA structure is moreover
132 compared to computational models of PlaC and PlaD to highlight similarities and differences between
133 these enzymes. Thus, we establish a link between structure and enzymatic function of PlaA.

134 **Results**

135 **PlaA displays a classical α/β-hydrolase fold containing the catalytic triad S30/D279/H282**

136 The gene for PlaA without the respective predicted N-terminal SP (amino acids 1-18) was expressed in
137 *E. coli* and purified via an N-terminal Strep-tag. After size exclusion chromatography (SEC), the protein
138 was subjected to crystallization. PlaA crystallized in spacegroup $P3_121$ with one chain of the monomeric
139 protein in the asymmetric unit. This crystal form differs from a previous report where PlaA has been
140 crystalized in space groups $P2_1$ and $P2_12_12_1$ but where structure determination has remained pending
141 (37). Initial phases were obtained from single-wavelength anomalous diffraction data collected at an X-
142 ray energy of 7 keV (wavelength = 1.7712 Å) of a crystal obtained in the presence of ammonium iodide
143 (Fig. S1A and B). Crystallization in the presence of 1-monopalmitoyllysophosphatidylcholine (16:0 LPC)
144 and avoiding polyethylene glycol (PEG) in the precipitant led to crystals of the same spacegroup (Fig.
145 S1A) and no significant structural differences were observed between the crystal structures determined
146 in this study. With the exception of a few residues at the N- and C-termini as well as parts of a highly
147 flexible surface loop (residues V91 – E97), the final structures show all of the PlaA protein (Fig. 1B). The
148 N-terminal Strep-tag was too flexible to produce traceable electron density. The highest resolution
149 obtained here is 1.45 Å for PlaA complexed with the 16:0 LPC hydrolysis product palmitate (Tab. 2). The
150 structures substantiate that PlaA is a canonical GDSL hydrolase with a typical α/β-hydrolase fold (Fig. 1B,
151 Fig. S1B). The catalytic triad was previously determined as S30, D279, H282 by means of mutational
152 analysis (27) and is confirmed in the 3D structure. The central β-sheet consists of five parallel β-strands
153 and is surrounded by a set of α-helices on both of its sides (Fig. 1B, Fig. S1C). The N-terminus and the C-
154 terminus of PlaA (shown in blue and red in Fig. 1B) are located in close proximity to each other.

155

156 **Detection of a hydrophobic channel that matches with linear fatty acids of 16 carbon atoms in close**
157 **proximity to the catalytic triad**

158 Interestingly, crystallization was initially only possible in the presence of PEG. Here, we observed
159 additional electron density in a hydrophobic channel in close proximity to the catalytic triad (Fig. S1D),
160 despite the fact that this channel is not accessible from the solvent. The channel has a length of approx.
161 20 Å, suggesting that the unexplained electron density derives from a molecule that mimics the fatty acid
162 moiety of the substrate such as short unbranched PEG components of the precipitant used to crystallize
163 the protein. We hence interpreted the additional electron density as a fragment of PEG. Subsequently,
164 we aimed for the structure of a complex of PlaA with its substrate 16:0 LPC by co-crystallization in a PEG-
165 free precipitant. This yielded crystals of the same space group (Fig. S1A) that diffracted to 1.45 Å

166 resolution. Here, we observed additional electron density that occupies the entire hydrophobic channel
167 (Fig. S1E). This density was interpreted as the product of PlaA-dependent hydrolysis of 16:0 LPC, palmitic
168 acid (Fig. 1C). Interestingly, no crystals were obtained in the absence of substrate (16:0 LPC) or product
169 analogues (palmitate, PEG), which may point towards higher flexibility of apo-PlaA. This flexibility may
170 include partial unfolding for hydrophobic substrate binding.
171

172 **A disulfide loop functions as a lid that covers the catalytic triad and reduces membrane interaction**
173 **before enzyme activation**

174 Regarding potential structural elements hindering substrate binding in the non-activated state of PlaA, a
175 disulfide loop (from C243 to C272; shown in orange in Fig. 1B and in yellow in Fig. 1D, respectively)
176 covers the entrance to the substrate binding pocket and the catalytic triad of PlaA. It is therefore
177 conceivable that ProA-mediated processing of the disulfide loop facilitates access of substrates to the
178 binding pocket and to the active site, explaining the increased LPLA activity upon exposure to ProA. The
179 previously determined preferred proteolytic maturation site E266/L267 at the C-terminal end of the lid
180 (27) is solvent accessible in the crystal structure (Fig. 1B, Fig. S1C). Parts of the lid display high B-factors,
181 indicating that they are relatively mobile. This flexibility may also explain why we found the hydrolysis
182 product palmitic acid bound to the active site (Fig. 1C and Fig. S1E) despite having crystallized uncleaved
183 PlaA. We propose that proteolytic maturation by ProA increases flexibility further and enables parts of
184 the lid to leave the position observed in the crystal structure. This would open up the entry to the active
185 site and is in line with proteolytic activation mechanisms of other lipases (38).
186

187 Among others, DALI (39) searches identify the cholin esterase ChoE from *P. aeruginosa* (PDB code 6uqv)
188 (40), the phospholipase PlpA from *Vibrio vulnificus* (PDB code 6jl2) (41), or the esterase domain of
189 autotransporter EstA from *P. aeruginosa* (PDB code 3kvn) (42) as highly structurally similar to PlaA (Fig.
190 2A-D). Interestingly, while these proteins also possess disulfide loops in similar positions, these disulfide
191 loops are shorter in sequence and they do not shield the active center as much as the disulfide loop of
192 PlaA in the unprocessed state observed here (Fig. 2A-D). As a consequence, the ligand binding sites of
193 these enzymes are solvent accessible, suggesting that they do not require proteolytic activation.
194

195 We further analyzed whether in addition to the previously shown increase in activity (27) also membrane
196 interaction of PlaA is influenced by disulfide loop processing and tested the catalytic inactive variant PlaA
197 S30N versus the respective mutant with truncated disulfide loop PlaA S30N Δaa248-267, in a Förster-

198 Resonance Energy Transfer (FRET) liposome-insertion assay. When protein-lipid interaction exceeds
199 peripheral binding and proteins at least insert into the lipid headgroup region, this leads to an increase in
200 the distance between the fluorophores and thus to reduced energy transfer. Consequently, the ratio of
201 donor and acceptor fluorescence intensities is a measure of protein insertion into membranes. This
202 effect is very prominent for antimicrobial peptides, like LL-37, and leads to a strong increase in the ratio
203 (43). For the disulfide loop mutant PlaA S30N ΔΔaa248-267 a concentration-dependent increase of the
204 ratio was as well detected and was higher compared to PlaA S30N with intact disulfide loop (Fig. 3).
205 However, the interaction of the disulfide loop mutant was less pronounced as noted for LL-37 (43). This
206 indicates that the PlaA disulfide loop mutant only inserts into the interface of the membrane. In
207 conclusion, our results show that the disulfide lid reduces lipid interaction; or in other words, lipid
208 interaction is facilitated by disulfide loop cleavage which might also impact enzyme activity.
209

210 **Substrate selectivity of PlaA concerning fatty acid chain length is governed by a molecular ruler**
211 **mechanism**

212 As mentioned above, we observed unexplained elongated electron density in the ligand binding site of
213 the first high-resolution structure of PlaA and attributed this to a PEG fragment deriving from the
214 precipitant solution (Fig. S1D). However, this molecule did not fill the binding site completely, and
215 further structural analysis suggested that PlaA can accommodate phospholipid substrates with linear
216 fatty acid chains of at least 16 carbon atoms length, which was then confirmed by the crystal structure of
217 PlaA in complex with palmitate (Fig. 1C, Fig. S1E). To further investigate the substrate spectrum of PlaA,
218 we tested whether LPLA activity of PlaA correlated with the length of the fatty acid chains. To this end,
219 PlaA was incubated with lysophosphatidylcholine (LPC) with diverse fatty acid residues. These varied in
220 length from eight to 22 carbon atoms. PlaA in its unprocessed form exhibited predominantly activity
221 towards 16:0 LPC (Fig. 4A, left side). Additionally, activity was compared to the disulfide loop-deleted
222 PlaA ΔAA248-67, which corresponds to ProA-processed PlaA (27). The LPLA activity of PlaA ΔAA248-67
223 was distinctly higher than that of untruncated PlaA and was mainly directed towards 16:0 and 14:0 LPC,
224 but 8:0 LPC, 12:0 LPC, and 18:0 LPC were also hydrolyzed to a lower extent (Fig. 4A, right side). As
225 hypothesized, no activity towards 20:0 LPC and 22:0 LPC was observed for both PlaA proteins. PlaA
226 variants with mutation of the catalytic serine Ser30 (PlaA S30N and PlaA S30N ΔAA248-67) were used as
227 controls and did not exhibit activity towards any of the tested lipid substrates (Fig. 4A, left and right side,
228 respectively). These findings suggest that the substrate selectivity of PlaA is governed by a molecular
229 ruler mechanism that measures the length of fatty acids by accommodating them to the ligand binding

230 site (44). To corroborate this, we mutated residue P283 pointing into the ligand binding site to leucine
231 (Fig. 1C and Fig. S2), hypothesizing that this larger residue would diminish the hydrophobic lipid binding
232 site and hence change the substrate preference of PlaA to lysophospholipids with shorter fatty acid
233 chains (Fig. 1C and Fig. S3). Indeed, although showing an overall reduced activity, PlaA P283L preferred
234 12:0 LPC over 14:0 and 16:0 LPC (Fig. 4B), highlighting the importance of the size of this ligand binding
235 site. In contrast, PlaA T220L where another residue in the binding site was mutated to leucine which
236 however did not point as much into the ligand binding site like P283L and accordingly did not show a
237 shift in the substrate preference (Fig. 4B and Fig. S2). In summary, our data suggest that substrate
238 preference with regard to fatty acid chain length is regulated by a ruler like mechanism.
239

240 **During growth of *L. pneumophila*, PlaA is first present in its unprocessed form until ProA is secreted**
241 PlaA is a type II-secreted protein found in culture supernatants of *L. pneumophila* (24,25,27). We were
242 interested if and when ProA-processing of PlaA occurs in *L. pneumophila* grown in liquid cultures. PlaA
243 was detected as ~33 kDa full-length protein (without signal peptide, protein sizes see Tab. 1) during lag
244 and logarithmic growth phases with a maximum quantity at 2 to 3 h of growth (Fig. 5A and B). During
245 mid-exponential growth, from ~4 h of incubation, processed PlaA with a molecular weight of ~25 kDa
246 was detected for the first time and from 5h remained the only PlaA version until late logarithmic /
247 stationary phase (Fig. 5A and 5B). These observations correlated with an accumulation of ProA in the
248 culture supernatants over time (Fig. 5C). In conclusion, our experiments indicate that PlaA, although
249 found in its full-length form in the culture supernatant at early growth phases, may not reach its full
250 activity before its processing at mid to late logarithmic growth phase. Full activity of PlaA may therefore
251 correlate to a later phase in bacterial growth and be associated with LCV and host cell exit of the
252 bacteria, as indicated previously (15).
253

254 **PlaA activation by ProA- is not inhibited by mutation of the preferred cleavage site E266/L267**
255 **highlighting broader cleavage site acceptance by ProA**
256 As outlined above, an important feature of PlaA is a disulfide loop lid structure. After its processing
257 access of lipid substrates to the catalytic active site and protein-lipid interaction is facilitated and thus
258 leads to an increase of LPLA activity. We previously reported that this disulfide loop is cleaved by ProA at
259 the preferred cleavage site E266/L267 in PlaA. Also, truncation of the disulfide loop in PlaA ΔAA248-67
260 yields more active PlaA and similar activity characteristics as ProA-processed PlaA (27). Subsequently, we
261 analyzed whether mutation of the main cleavage site E266/L267 may hinder PlaA activation. We found

262 that the mutation of E266 and L267 into N266 and N267, respectively, is not sufficient to prevent ProA-
263 dependent increase in LPLA activity of PlaA and its proteolytic processing. Specifically, similar activities
264 were detected for PlaA and the E266N L267N mutant and similar processing to the smaller version of
265 PlaA by ProA (Fig. 5D and 5E). The respective catalytic inactive S30N controls did not show activity (Fig.
266 5D). This indicates that ProA may attack other exposed residues surrounding the major cleavage site
267 E266/L267 in the disulfide loop and lead to PlaA processing and activation. This was already implied by
268 peptide mapping of ProA-digested PlaA which identified additional but less preferred cleavage sites, such
269 as K264/P265, P265/E266, and L267/T268, directly upstream and downstream of E266/L267 (27). These
270 observations further highlight the previously described broad cleavage site acceptance by ProA in other
271 substrates (45).
272

273 **Comparison of PlaA to structural models of PlaC and PlaD highlights the presence of disulfide loops**
274 **shielding the catalytic side in PlaC but not PlaD.**

275 To obtain additional insight into the structure of the three *L. pneumophila* GSDL phospholipases, we
276 generated structural models of PlaC and PlaD using the template-free routine of AlphaFold (46). The
277 structure of PlaA was predicted as well to evaluate the method, and no significant differences were
278 found with respect to the X-ray structures described above (Fig. 6A, Fig. S3A-C). Notably, this also
279 includes the more flexible parts of PlaA (residues V91 – E97 and the disulfide loop), whose flexibility is
280 correctly indicated by a lower confidence score. Importantly, the predicted conformation of the disulfide
281 loop matches the crystal structure very well (Fig. S3A-C).
282

283 Compared to PlaA, PlaC although similar in structure is predicted to contain additional helical elements
284 in P57 – G120 and D166 – P193 which correspond to its larger size (Fig. 6B). Of these, the second region
285 replaces the flexible region V91 – D95 of PlaA. Similar to PlaA, PlaC has a lid domain that is delimited by a
286 disulfide bridge (C343-C388) which accommodates the proteolytic maturation site (26) . In PlaC, this lid
287 includes an α-helix (362-370) that shields the active site from the solvent. However, this α-helix is slightly
288 shifted away from the active site, resulting in a larger entrance funnel for PlaC possibly explaining
289 differences in the substrate specificity of both enzymes. While PlaA preferentially hydrolyzes
290 lysophospholipids, PlaC also accepts larger substrates such as diacyl phospholipids (26). The length of
291 PlaC's hydrophobic substrate channel is identical to PlaA's, indicating that in both cases linear fatty acids
292 with ~16 carbon atoms are the preferred substrates.
293

294 The structure of PlaD includes the α/β hydrolase domain (N-terminal domain) and is predicted to have an
295 additional α-helical domain of unknown function at its C-terminus (P403 – T516) (Fig. 6C). The relative
296 orientation towards the α/β-hydrolase domain is unclear at present since both domains are connected
297 by a long flexible linker (P371 - L402). Comparison with PlaA reveals additional helical elements (e.g. P60
298 – P72). Importantly, PlaD does not contain a disulfide loop, and the respective region of the protein
299 (Y311 – A334, shown in light blue in Fig. 6C) is predicted to adopt an open conformation that leads to an
300 unshielded substrate binding site. In addition to differences in protein secretion, these features may
301 explain further possible differences in the activation mechanism of this protein compared to PlaA and
302 PlaC. The length of the hydrophobic substrate channel of PlaD, on the other hand, is identical to that of
303 PlaA, again suggesting preference for linear fatty acids with ~16 carbon atoms.

304 **Discussion**

305

306 Here we show that PlaA, which is one of three proteins of the GDSL phospholipase family found in *L.*
307 *pneumophila* (19), adopts an α/β hydrolase fold typically found in similar enzymes of other bacteria, such
308 as the cholin esterase ChoE from *Pseudomonas aeruginosa* (PDB code 6uqv), the phospholipase PlpA
309 from *Vibrio vulnificus* (PDB code 6jl2) or the esterase domain of autotransporter EstA from *P. aeruginosa*
310 (PDB code 3kvn) to name just a few examples (Fig. 2). However, PlaA also shows specific features which
311 relate to its activation mechanism and substrate specificity. Structural analysis reveals that a disulfide
312 loop lid structure reduces substrate access to the catalytic site in ProA-unprocessed PlaA. The active site
313 gets more accessible when the disulfide loop is opened up by proteolysis. After structural modelling
314 using AlphaFold, a similar activation mechanism is suggested for PlaC and cleavage of the disulfide loop
315 and PlaC activation by ProA was previously shown (26) but is not suggested for PlaD, where the catalytic
316 site seemed freely accessible as further observed in ChoE, PlpA, and EstA (Fig. 2).

317

318 Lid structures are very common in lipases and are important for substrate specificity and control of
319 enzymatic activity (47). It can be assumed that processing of the PlaA disulfide loop by ProA might
320 completely remove the lid or at least increase its flexibility. This might affect the conformation of the
321 active site or the potential substrate-binding domain or both. It is conceivable that the access of lipid
322 substrates to the active site channel of PlaA is facilitated by the structural alterations induced by ProA-
323 dependent processing, which might explain the increased LPLA activity of processed PlaA. Proteolytic
324 processing is a common mechanism for activation of enzymes that have been produced as inactive
325 zymogens (38). Among others, the induction of enzymatic activity after processing within a disulfide loop
326 has been shown for some, such as *Pseudomonas* exotoxin A and Shiga toxin from enterohemorrhagic
327 *Escherichia coli* (48-51). Although unprocessed PlaA is not completely inactive, it can be assumed that
328 the rationale of ProA-dependent regulation of PlaA is to increase the enzymatic activity only after PlaA is
329 secreted to the exterior and at the required time point. Since phospholipase activities are potentially
330 harmful to the bacterium itself, we propose that the here presented activation mechanism is also used
331 to avoid self-inflicted lysis from a lytic enzyme before secretion.

332

333 *L. pneumophila* is an intracellularly replicating lung pathogen which induces major lung damage leading
334 to a severe pneumonia and the secreted bacterial phospholipases may contribute to the clinical picture
335 (2,19). Eukaryotic membranes and the surfactant phospholipid monolayer in the lung contain major
336 amounts of phospholipids with esterified fatty acids of a length of ~16 carbon atoms (52). We showed

337 that the size of an intramolecular channel in PlaA, PlaC, and PlaD nicely fits to harbor such lipids and also
338 the reaction product palmitic acid (Fig. 1C) which mechanistically underlines host-adapted substrate
339 specificity of these enzymes.
340
341 Interestingly, it was shown that PlaA is responsible for the destabilization of the replication vacuole in
342 the absence of the T4BSS secreted effector SdhA, which localizes to the LCV (15). The LCV protective
343 mechanism of SdhA has recently been shown as binding and blocking the function of OCRL
344 (OculoCerebroRenal syndrome of Lowe), an inositol 5-phosphatase pivotal for controlling endosomal
345 dynamics and participating in vacuole disruption (28). It is important for intracellular pathogens like
346 *Legionella* to maintain the integrity of the replication vacuole for the period of bacterial propagation to
347 avoid detection by the immune system of the host (55). However, for the exit of the pathogen and the
348 initiation of a new infection cycle, the vacuole needs to be disrupted (16). Assuming that the functions of
349 SdhA and PlaA are opposed and must be balanced for maintenance of the LCV integrity for bacterial
350 replication (55), it may be that a change of abundance or activity of either factor could result in exit of *L.*
351 *pneumophila*. The here addressed increase of PlaA activity and membrane interaction by proteolytic
352 processing could disturb the balance between SdhA and PlaA in an infection and might thus lead to
353 destabilization of the LCV triggering the exit process.
354
355 Our analyses of culture supernatants at multiple time points during *L. pneumophila* growth in liquid
356 medium revealed that PlaA is initially secreted as full-length protein. Processing was first detected during
357 mid-exponential growth when ProA quantities increased. We speculate that ProA-processing of PlaA
358 does not occur before a critical density of intravacuolar bacteria is reached which produces sufficient
359 ProA quantities. This might happen in similarity to the regulatory process of quorum sensing (56). In
360 parallel, proteolytic activation of PlaC might be additionally triggered which might allow cooperation of
361 PlaC, majorly revealing PLA activity, and PlaA, majorly possessing LPLA activity. Thus, destabilization of
362 the LCV for host exit can be linked to coordinated activation of several enzyme activities at high cell
363 density and completed bacterial replication.
364
365 In summary, these findings provide insight into the relationship between structure and activity of PlaA
366 and for the other GSDL hydrolases in *L. pneumophila*. We found that these enzymes possess structural
367 features that may lead to a specific activity and activation profile tailored to the needs of the bacterium.
368

369 **Experimental procedures**

370

371 **Bacterial strains and growth conditions**

372 All experiments and sequence or structure predictions were performed with *L. pneumophila* sg1 strain
373 Corby including recombinant gene expression in *E. coli* BL21. The strains used and generated in the study
374 are listed in Tab. 3. *L. pneumophila* strains were grown on buffered charcoal yeast extract (BCYE) agar
375 and in buffered yeast extract (BYE) broth and *E. coli* strains were grown on Luria Bertani (LB) agar and in
376 LB broth as described previously (36,57,58). If appropriate, 100 µg/ml ampicillin or 50 µg/ml kanamycin
377 were added to the *E. coli* cultures.

378

379 **Construction of plasmids**

380 The vector pMH42 was generated from pMH41 by means of the QuikChange Site-Directed Mutagenesis
381 Kit (Stratagene) using the primers PlaA_S30N_fw (5'-GTATTTGGTGATAATTTGTCGGATAACGG-3') and PlaA
382 S30N_rv (5'-CCGTTATCCGACAAATTATCACCAAATAC-3') for introduction of the S30N point mutation in
383 *plaA* (Tab. 3). The vectors pUS8 and pUS9 were generated from pCL119 using the primer pairs
384 plaA_P283L_fw/rv (5'- GATTTGGTTCATCTGACAGCG-*3'/%'- CGCTGTCAGATGAACCAAATC-3') and
385 plaA_P220L_fw/rv (5'-GACTTGGGTAGTCATTTTGACC-3'/ 5'-GACTACCCAAGTCAAAAAACAAC-3'),
386 respectively (Tab. 3). Primers were obtained from Eurofins MWG Operon and Integrated DNA
387 Technologies. All restriction enzymes were obtained from New England Biolabs. Plasmid DNA was
388 introduced into *E. coli* by heat shock transformation.

389

390 **Expression and purification of recombinant PlaA or ProA for enzyme activity tests and analysis of**
391 **crystal structure**

392 *E. coli* BL21 strains harboring plasmids for recombinant expression of *plaA* variants without SP and N-
393 terminally fused Strep-tag (Tab. 3) were grown in LB broth supplemented with ampicillin at 37 °C and
394 250 rpm to an OD_{600} = 0.8, induced with 0.1 mM IPTG, and transferred to 18 °C and 250 rpm for 16 – 17
395 h. The bacterial pellet was collected and resuspended in 100 mM Tris-HCl, pH 8.0, containing 100 mM
396 NaCl. Homogenization was performed with Emulsi Flex C3 (Avestin) applying 25,000 to 30,000 psi. The
397 soluble fraction was collected by centrifugation at 13,000 g and 4 °C for 60 min. Strep-PlaA and variants
398 were purified using Strep-Tactin Superflow high capacity resin (IBA) and further purified by SEC
399 (Superdex S200 10/30 Increase) performed with SEC buffer (20 mM Tris pH 8, 150 mM NaCl, 1 mM DTT)

400 according to the manufacturer's instructions. Recombinant periplasmic ProA was isolated by osmotic
401 shock from *E. coli* BL21 (pCL15) and subsequent anion exchange chromatography (26).
402

403 **Crystallization, X-ray diffraction, and structure determination**

404 Crystals were obtained by sitting drop vapor diffusion at 20 °C. Initially, 200 nl PlaA solution at 8 mg/mL
405 in SEC buffer were mixed with 200 nl of 14.7% (w/v) PEG3350, 1% (w/v) PEG 1K, 0.5% (w/v) PEG200,
406 8.9% (v/v) tacsimate pH 5, 200 mM NH_4I, 1 mM $CaCl_2$, and 1 mM $MgCl_2$. For cryoprotection, crystals were
407 briefly washed in a solution of 10% (v/v) (2R,3R)-(−)-2,3-butandiole, 16% (w/v) PEG3350, 6% (v/v)
408 Tacsimate pH 5, and 920 mM NH_4I. To exploit the f'/f'' difference arising from the L I absorption edge of
409 iodine (5.1881 keV, 2.3898 Å), two datasets at an X-ray energy of 7.000 keV (λ = 1.771196 Å) and with
410 detector distances of 140 mm and 135 mm were collected at beamline X06DA (PXIII) of the Swiss Light
411 Source (SLS; Villigen, Switzerland) (59). These data were indexed, scaled and merged with autoproc (60)
412 and then used for initial phasing by single anomalous dispersion (SAD) analysis through hkl2map and the
413 SHELX-package (61) The resulting poly-alanine model served as a template for phenix.autobuild (62).
414 Manual editing was done in Coot (63) from the CCP4 software suite (64). Structure refinement was done
415 with phenix.refine and pdb-redo (65,66). 13 iodide anions were placed in the final model (Fig. S1B).
416 High resolution data of a crystal obtained under similar conditions were collected at the same beamline,
417 using an X-ray wavelength of 1.3778 Å. Diffraction data of a crystal grown from 7 mg/mL PlaA solution in
418 SEC buffer supplemented with 500 µM 1-monopalmitoyllysophosphatidylcholine (16:0 LPC) with a
419 precipitant consisting of 2.2 M $(NH_4)_2SO_4$ and 0.2 M NH_4-acetate were collected on beamline P11 of the
420 PETRAIII synchrotron (DESY Hamburg, Germany) (67). The cryoprotectant consisted of precipitant
421 solution supplemented with 10% (v/v) (2R,3R)-(−)-2,3-butandiole in this case. Refinement proceeded via
422 Fourier synthesis followed by employing the same methods as in the case for the SAD structure (specific
423 data see Tab. 2).
424

425 **Prediction of 3D structures of PlaA, PlaC and PlaD**

426 The 3D structures of PlaA (gene lpc1811), PlaC (gene lpc3121) und PlaD (gene lpc0558) of *L. pneumophila*
427 Corby were predicted using the template-less routine of AlphaFold (46) through a local installation of
428 ColabFold (68). The required protein sequences were obtained from the NCBI protein database (PlaA:
429 WP_011947186.1; PlaC: WP_011947718.1; PlaD: WP_011947511.1).
430

431 **Preparation of cell lysates**

432 Pellets of 1 ml overnight cultures of strains expressing PlaA and PlaA variants were lysed with 0.5 mg/ml
433 lysozyme, 1% Triton X-100 in 1 ml 40 mM Tris-HCl buffer and supplemented with 6 mM NaN_3.
434

435 ***In vitro* analysis of lipolytic activity and proteolytic processing of recombinant PlaA**

436 Lipolytic activities of recombinant PlaA variants were investigated as described previously (25,36,69). The
437 lipid substrates 1-monooctanoyllysophosphatidylcholine (8:0 LPC), 1-
438 monolauroyllysophosphatidylcholine (12:0 LPC), monotetradecanoyllysophosphatidylcholine (14:0 LPC),
439 1-monopalmitoyllysophosphatidylcholine (16:0 LPC), 1-monostearoyllysophosphatidylcholine (18:0 LPC),
440 1-monoarachidoyllysophosphatidylcholine (20:0 LPC), and 1-monobehenoyllysophosphatidylcholine
441 (22:0 LPC) purchased from Avanti Polar Lipids (Alabaster, AL, USA) were applied for the assays. Briefly,
442 purified recombinant proteins or cell lysates expressing recombinant protein were incubated with
443 6.7 mM lipid suspensions as micelles (in 40 mM Tris-HCl, 1% Triton X-100) with or without addition of
444 3.5 mU ProA at 37 °C for the indicated time followed by quantitative detection of free fatty acids (FFA) by
445 means of the NEFA-C kit (WAKO Chemicals, Neuss, Germany) according to the instructions of the
446 manufacturer.

447 **FRET liposome-interaction assay**

448 Insertion of PlaA proteins into liposome membranes was determined in 40 mM Tris, 150 mM NaCl, pH
449 7.5, at 37 °C by FRET spectroscopy applied as a probe dilution assay (70). L-α-phosphatidylcholine (ePC,
450 95%, chicken egg) and L-α-phosphatidylethanolamine (ecPE, *E. coli*) were purchased from Avanti (Avanti
451 Polar Lipids Inc., Alabaster, AL, USA) and prepared at stock concentrations of 10 mg/mL in $CHCl_3$.
452 Fluorescence conjugated lipids *N*-(7-nitrobenz-2-oxa-1,3-diazol-4-yl)-
453 1,2-dihexadecanoyl-*sn*-glycero-3-phosphoethanolamine (NBD-PE) and Lissamine™ Rhodamine B
454 1,2-dihexadecanoyl-*sn*-glycero-3-phosphoethanolamine (Rho-DHPE), were purchased from Life
455 Technologies (Carlsbad, CA, USA). Proteins were added to PC:PE (1:1) liposomes, which were labelled
456 with 1% of the donor NBD-PE and 1% of the acceptor rhodamine-PE. The fluorescence was measured by
457 means of a spectrometer (Fluorolog 3, Horiba Jobin Yvon GmbH, Bensheim, Germany). NBD excitation
458 wavelength was 470 nm. Protein insertion was monitored as the increase of the ratio of the donor
459 fluorescence intensity I_{donor} at 531 nm to that of the acceptor intensity $I_{acceptor}$ at 593 nm in a
460 concentration dependent manner. This ratio depends on the Förster efficiency; therefore, a ratio > 1
461 highlights that the mean distance of donor and acceptor dyes increased. Values were determined 5 min
462 after addition of 1, 5, 10, 30, 50, and 100 µg/ml protein. Buffer (see above) was used to dilute the
463 proteins and control.

464

465 **Analysis of processing status of PlaA from *L. pneumophila***

466 Overnight cultures of *L. pneumophila* sg1 strain Corby grown in buffered yeast extract (BYE) broth were
467 washed once with warm BYE broth to remove secreted proteins, adjusted to $OD_{600} = 0.3$ in 37 °C BYE
468 broth and incubated for 8 h at 37 °C and 250 rpm. OD_{600} was measured hourly, aliquots of the cultures
469 were adjusted to $OD_{600} = 0.1$ and supernatants were concentrated 100-fold by trichloroacetic acid
470 precipitation. For processing analysis of PlaA by ProA, 250ng PlaA or PlaA E266N L267N were incubated
471 with 0.5 mM ProA for 10-60 min at 37°C. These samples were analyzed in Western blots with primary
472 polyclonal rabbit antibodies against PlaA and ProA (generated by BioGenes from recombinant proteins)
473 (27).

474

475 **Figure preparation**

476 Figures were prepared with Microsoft Power Point 2010 and Inkscape 0.92. All images, symbols and
477 fonts within the figures are acquired from Microsoft Power Point 2010. Images of crystal structures were
478 generated with PyMOL (71). Western Blots were labelled and processed with Adobe Photoshop CS6.
479 Graphs included in the Figures are visualized by Microsoft Excel 2010.

480

481 **Data availability statement**

482 All data generated or analyzed during this study are included in this published article or in the
483 supplementary information. Structures are available at PDBe with the accession codes 8A24 (PlaA iodide
484 SAD), 8A25 (PlaA complex with PEG fragment), and 8A26 (PlaA complex with palmitate).

485

486 **Supporting information**

487 This article contains supporting information.

488

489 **Acknowledgements**

490 We thank Susanne Karste, Ute Strutz, and Christian Galisch (Robert Koch-Institut) and Sabrina Groth
491 (Research Center Borstel) for excellent technical assistance. AF, TG, and WB, received funding from the
492 German Research Association (DFG) (FL359/6-1/2; priority program SPP2225 Exit Strategies of
493 Intracellular Pathogens FL359/10-1 and GU568/8-1; 281361126/GRK2223). We acknowledge the staff at
494 beamlines PXIII/X06DA at SLS (Paul Scherrer Institute, Villigen, Switzerland) and P11 (PETRAIII, DESY
495 Hamburg, Germany) for providing access to their facilities.

496

497 **Authors contributions**

498 conceptualized the study: M.H., M.D., C.L., W.B., A.F.

499 supervised the study: W.B., A.F.

500 conceived and designed the experiments: M.H., M.D., S.W., C.L., W.B., A.F., T.G.

501 acquired data: M.H., M.D., S.W., C.L.

502 conducted the experiments: M.H., M.D., S.W., C.L.

503 analyzed the data: M.H., M.D., S.W., C.L., W.B., A.F., T.G.

504 interpreted the results: M.H., M.D., S.W., C.L., W.B., A.F., T.G.

505 drafted the manuscript: M.H., M.D., W.B., A.F.

506 revised the manuscript: M.H., M.D., S.W., C.L., W.B., A.F., T.G.

507 approved the final version: M.H., M.D., S.W., C.L., W.B., A.F., T.G.

508

509 **Data sharing**

510 All data generated or analyzed during this study are available in this article and the appendices.

511

512 **Declaration of Interests**

513 The authors declare that they have no conflicts of interest with the contents of this article.

514

515

516

517

518 **References**

519 1. Fields, B. S. (1996) The molecular ecology of legionellae. *Trends Microbiol.* **4**, 286-290
520 2. Mondino, S., Schmidt, S., Rolando, M., Escoll, P., Gomez-Valero, L., and Buchrieser, C. (2020)
521 Legionnaires' Disease: State of the Art Knowledge of Pathogenesis Mechanisms of Legionella.
522 3. Horwitz, M. A. (1983) The Legionnaires' disease bacterium (Legionella pneumophila) inhibits
523 phagosome-lysosome fusion in human monocytes. *The Journal of Experimental Medicine* **158**,
524 2108-2126
525 4. Finsel, I., and Hilbi, H. (2015) Formation of a pathogen vacuole according to Legionella
526 pneumophila: how to kill one bird with many stones. *Cell. Microbiol.* **17**, 935-950
527 5. Isberg, R. R., O'connor, T. J., and Heidtman, M. (2009) The Legionella pneumophila replication
528 vacuole: making a cosy niche inside host cells. *Nature Reviews Microbiology* **7**, 13-24
529 6. Segal, G., Purcell, M., and Shuman, H. A. (1998) Host cell killing and bacterial conjugation require
530 overlapping sets of genes within a 22-kb region of the Legionella pneumophila genome. *Proc.*
531 *Natl. Acad. Sci. U. S. A.* **95**, 1669-1674
532 7. Cianciotto, N. P. (2009) Many substrates and functions of type II secretion: lessons learned from
533 Legionella pneumophila. *Future Microbiol.* **4**, 797-805
534 8. White, R. C., and Cianciotto, N. P. (2019) Assessing the impact, genomics and evolution of type II
535 secretion across a large, medically important genus: the Legionella type II secretion paradigm.
536 *Microbial genomics* **5**
537 9. Burstein, D., Amaro, F., Zusman, T., Lifshitz, Z., Cohen, O., Gilbert, J. A., Pupko, T., Shuman, H. A.,
538 and Segal, G. (2016) Genomic analysis of 38 Legionella species identifies large and diverse
539 effector repertoires. *Nat. Genet.* **48**, 167
540 10. Gomez-Valero, L., Rusniok, C., Carson, D., Mondino, S., Pérez-Cobas, A. E., Rolando, M., Pasricha,
541 S., Reuter, S., Demirtas, J., and Crumbach, J. (2019) More than 18,000 effectors in the Legionella
542 genus genome provide multiple, independent combinations for replication in human cells.
543 *Proceedings of the National Academy of Sciences* **116**, 2265-2273
544 11. Gaspar, A. H., and Machner, M. P. (2014) VipD is a Rab5-activated phospholipase A1 that
545 protects Legionella pneumophila from endosomal fusion. *Proc. Natl. Acad. Sci. U. S. A.* **111**, 4560-
546 4565
547 12. VanRheenen, S. M., Luo, Z. Q., O'Connor, T., and Isberg, R. R. (2006) Members of a Legionella
548 pneumophila family of proteins with ExoU (phospholipase A) active sites are translocated to
549 target cells. *Infect. Immun.* **74**, 3597-3606
550 13. Shohdy, N., Efe, J. A., Emr, S. D., and Shuman, H. A. (2005) Pathogen effector protein screening in
551 yeast identifies Legionella factors that interfere with membrane trafficking. *Proc. Natl. Acad. Sci.*
552 *U. S. A.* **102**, 4866-4871
553 14. Li, X., Anderson, D. E., Chang, Y. Y., Jarnik, M., and Machner, M. P. (2022) VpdC is a ubiquitin-
554 activated phospholipase effector that regulates Legionella vacuole expansion during infection.
555 *Proc. Natl. Acad. Sci. U. S. A.* **119**, e2209149119
556 15. Creasey, E. A., and Isberg, R. R. (2012) The protein SdhA maintains the integrity of the Legionella-
557 containing vacuole. *Proc. Natl. Acad. Sci. U. S. A.* **109**, 3481-3486
558 16. Flieger, A., Frischknecht, F., Hacker, G., Hornef, M. W., and Pradel, G. (2018) Pathways of host
559 cell exit by intracellular pathogens. *Microb Cell* **5**, 525-544
560 17. Striednig, B., Lanner, U., Niggli, S., Katic, A., Vormittag, S., Brulisauer, S., Hochstrasser, R., Kaech,
561 A., Welin, A., Flieger, A., Ziegler, U., Schmidt, A., Hilbi, H., and Personnic, N. (2021) Quorum
562 sensing governs a transmissive Legionella subpopulation at the pathogen vacuole periphery.
563 *EMBO Rep* **22**, e52972

564 18. Flores-Diaz, M., Monturiol-Gross, L., Naylor, C., Alape-Giron, A., and Flieger, A. (2016) Bacterial
565 Sphingomyelinases and Phospholipases as Virulence Factors. *Microbiol. Mol. Biol. Rev.* **80**, 597-
566 628
567 19. Hiller, M., Lang, C., Michel, W., and Flieger, A. (2018) Secreted phospholipases of the lung
568 pathogen Legionella pneumophila. *Int. J. Med. Microbiol.* **308**, 168-175
569 20. Lang, C., and Flieger, A. (2011) Characterisation of Legionella pneumophila phospholipases and
570 their impact on host cells. *Eur. J. Cell Biol.* **90**, 903-912
571 21. Diwo, M., Michel, W., Aurass, P., Kuhle-Keindorf, K., Pippel, J., Krausze, J., Wamp, S., Lang, C.,
572 Blankenfeldt, W., and Flieger, A. (2021) NAD(H)-mediated tetramerization controls the activity of
573 Legionella pneumophila phospholipase PlaB. *Proc. Natl. Acad. Sci. U. S. A.* **118**
574 22. Akoh, C. C., Lee, G.-C., Liaw, Y.-C., Huang, T.-H., and Shaw, J.-F. (2004) GDSL family of serine
575 esterases/lipases. *Prog. Lipid Res.* **43**, 534-552
576 23. Upton, C., and Buckley, J. T. (1995) A new family of lipolytic enzymes? *Trends Biochem. Sci.* **20**,
577 178-179
578 24. Flieger, A., Gong, S., Faigle, M., Stevanovic, S., Cianciotto, N. P., and Neumeister, B. (2001) Novel
579 lysophospholipase A secreted by Legionella pneumophila. *J. Bacteriol.* **183**, 2121-2124
580 25. Flieger, A., Neumeister, B., and Cianciotto, N. P. (2002) Characterization of the gene encoding the
581 major secreted lysophospholipase A of Legionella pneumophila and its role in detoxification of
582 lysophosphatidylcholine. *Infect. Immun.* **70**, 6094-6106
583 26. Lang, C., Rastew, E., Hermes, B., Siegbrecht, E., Ahrends, R., Banerji, S., and Flieger, A. (2012) Zinc
584 metalloproteinase ProA directly activates Legionella pneumophila PlaC
585 glycerophospholipid:cholesterol acyltransferase. *J. Biol. Chem.* **287**, 23464-23478
586 27. Lang, C., Hiller, M., and Flieger, A. (2017) Disulfide loop cleavage of Legionella pneumophila PlaA
587 boosts lysophospholipase A activity. *Sci. Rep.* **7**, 16313
588 28. Choi, W. Y., Kim, S., Aurass, P., Huo, W., Creasey, E. A., Edwards, M., Lowe, M., and Isberg, R. R.
589 (2021) SdhA blocks disruption of the Legionella-containing vacuole by hijacking the OCRL
590 phosphatase. *Cell Rep* **37**, 109894
591 29. Flieger, A., Gong, S., Faigle, M., Northoff, H., and Neumeister, B. (2001) In vitro secretion kinetics
592 of proteins from Legionella pneumophila in comparison to proteins from non-pneumophila
593 species. *Microbiology* **147**, 3127-3134
594 30. Aurass, P., Gerlach, T., Becher, D., Voigt, B., Karste, S., Bernhardt, J., Riedel, K., Hecker, M., and
595 Flieger, A. (2016) Life Stage-specific Proteomes of Legionella pneumophila Reveal a Highly
596 Differential Abundance of Virulence-associated Dot/Icm effectors. *Mol. Cell. Proteomics* **15**, 177-
597 200
598 31. White, R. C., Gunderson, F. F., Tyson, J. Y., Richardson, K. H., Portlock, T. J., Garnett, J. A., and
599 Cianciotto, N. P. (2018) Type II Secretion-Dependent Aminopeptidase LapA and Acyltransferase
600 PlaC Are Redundant for Nutrient Acquisition during Legionella pneumophila Intracellular
601 Infection of Amoebas. *MBio* **9**
602 32. Dekker, N. (2000) Outer-membrane phospholipase A: known structure, unknown biological
603 function: MicroReview. *Mol. Microbiol.* **35**, 711-717
604 33. Kuhle, K., Krausze, J., Curth, U., Rossle, M., Heuner, K., Lang, C., and Flieger, A. (2014)
605 Oligomerization inhibits Legionella pneumophila PlaB phospholipase A activity. *J. Biol. Chem.*
606 **289**, 18657-18666
607 34. Bleffert, F., Granzin, J., Caliskan, M., Schott-Verdugo, S. N., Siebers, M., Thiele, B., Rahme, L.,
608 Felgner, S., Dormann, P., Gohlke, H., Batra-Safferling, R., Jaeger, K. E., and Kovacic, F. (2022)
609 Structural, mechanistic, and physiological insights into phospholipase A-mediated membrane
610 phospholipid degradation in Pseudomonas aeruginosa. *Elife* **11**
611 35. Aurass, P., Schlegel, M., Metwally, O., Harding, C. R., Schroeder, G. N., Frankel, G., and Flieger, A.
612 (2013) The Legionella pneumophila Dot/Icm-secreted effector PlcC/CegC1 together with PlcA

613 and PlcB promotes virulence and belongs to a novel zinc metallophospholipase C family present
614 in bacteria and fungi. *J. Biol. Chem.* **288**, 11080-11092
615 36. Banerji, S., Bewersdorff, M., Hermes, B., Cianciotto, N. P., and Flieger, A. (2005) Characterization
616 of the major secreted zinc metalloprotease- dependent glycerophospholipid:cholesterol
617 acyltransferase, PlaC, of Legionella pneumophila. *Infect. Immun.* **73**, 2899-2909
618 37. Qu, X., Song, X., Zhang, N., Ma, J., and Ge, H. (2020) The phospholipase A effector PlaA from
619 Legionella pneumophila: expression, purification and crystallization. *Acta Crystallogr F Struct Biol*
620 *Commun* **76**, 138-144
621 38. Vanaman, T. C., and Bradshaw, R. A. (1999) Proteases in cellular regulation minireview series. *J.*
622 *Biol. Chem.* **274**, 20047-20047
623 39. Holm, L. (2020) DALI and the persistence of protein shape. *Protein Sci.* **29**, 128-140
624 40. Pham, V. D., To, T. A., Gagne-Thivierge, C., Couture, M., Lague, P., Yao, D., Picard, M. E., Lortie, L.
625 A., Attere, S. A., Zhu, X., Levesque, R. C., Charette, S. J., and Shi, R. (2020) Structural insights into
626 the putative bacterial acetylcholinesterase ChoE and its substrate inhibition mechanism. *J. Biol.*
627 *Chem.* **295**, 8708-8724
628 41. Wan, Y., Liu, C., and Ma, Q. (2019) Structural analysis of a Vibrio phospholipase reveals an
629 unusual Ser-His-chloride catalytic triad. *J. Biol. Chem.* **294**, 11391-11401
630 42. van den Berg, B. (2010) Crystal Structure of a Full-Length Autotransporter. *J. Mol. Biol.* **396**, 627-
631 633
632 43. de Miguel Catalina, A., Forbrig, E., Kozuch, J., Nehls, C., Paulowski, L., Gutsmann, T., Hildebrandt,
633 P., and Mroginski, M. A. (2019) The C-Terminal VPRTES Tail of LL-37 Influences the Mode of
634 Attachment to a Lipid Bilayer and Antimicrobial Activity. *Biochemistry* **58**, 2447-2462
635 44. Anso, I., Basso, L. G. M., Wang, L., Marina, A., Paez-Perez, E. D., Jager, C., Gavotto, F., Tersa, M.,
636 Perrone, S., Contreras, F. X., Prandi, J., Gilleron, M., Linster, C. L., Corzana, F., Lowary, T. L.,
637 Trastoy, B., and Guerin, M. E. (2021) Molecular ruler mechanism and interfacial catalysis of the
638 integral membrane acyltransferase PatA. *Sci Adv* **7**, eabj4565
639 45. Scheithauer, L., Thiem, S., Schmelz, S., Dellmann, A., Bussow, K., Brouwer, R., Unal, C. M.,
640 Blankenfeldt, W., and Steinert, M. (2021) Zinc metalloprotease ProA of Legionella pneumophila
641 increases alveolar septal thickness in human lung tissue explants by collagen IV degradation. *Cell.*
642 *Microbiol.* **23**, e13313
643 46. Jumper, J., Evans, R., Pritzel, A., Green, T., Figurnov, M., Ronneberger, O., Tunyasuvunakool, K.,
644 Bates, R., Žídek, A., Potapenko, A., Bridgland, A., Meyer, C., Kohl, S. A. A., Ballard, A. J., Cowie, A.,
645 Romera-Paredes, B., Nikolov, S., Jain, R., Adler, J., Back, T., Petersen, S., Reiman, D., Clancy, E.,
646 Zielinski, M., Steinegger, M., Pacholska, M., Berghammer, T., Bodenstein, S., Silver, D., Vinyals,
647 O., Senior, A. W., Kavukcuoglu, K., Kohli, P., and Hassabis, D. (2021) Highly accurate protein
648 structure prediction with AlphaFold. *Nature* **596**, 583-589
649 47. Khan, F. I., Lan, D., Durrani, R., Huan, W., Zhao, Z., and Wang, Y. (2017) The Lid Domain in
650 Lipases: Structural and Functional Determinant of Enzymatic Properties. *Frontiers in*
651 *bioengineering and biotechnology* **5**, 16-16
652 48. Gordon, V. M., and Leppla, S. H. (1994) Proteolytic activation of bacterial toxins: role of bacterial
653 and host cell proteases. *Infect. Immun.* **62**, 333-340
654 49. Kurmanova, A., Llorente, A., Polesskaya, A., Garred, Ø., Olsnes, S., Kozlov, J., and Sandvig, K.
655 (2007) Structural requirements for furin-induced cleavage and activation of Shiga toxin. *Biochem.*
656 *Biophys. Res. Commun.* **357**, 144-149
657 50. Ogata, M., Fryling, C., Pastan, I., and FitzGerald, D. (1992) Cell-mediated cleavage of
658 Pseudomonas exotoxin between Arg279 and Gly280 generates the enzymatically active fragment
659 which translocates to the cytosol. *J. Biol. Chem.* **267**, 25396-25401
660 51. van Deurs, B., and Sandvig, K. (1995) Furin-induced cleavage and activation of Shiga toxin. *J. Biol.*
661 *Chem.* **270**, 10817-10821

662 52. Veldhuizen, R., Nag, K., Orgeig, S., and Possmayer, F. (1998) The role of lipids in pulmonary
663 surfactant. *Biochim. Biophys. Acta* **1408**, 90-108
664 53. Laguna, R. K., Creasey, E. A., Li, Z., Valtz, N., and Isberg, R. R. (2006) A Legionella pneumophila-
665 translocated substrate that is required for growth within macrophages and protection from host
666 cell death. *Proceedings of the National Academy of Sciences* **103**, 18745-18750
667 54. Ruiz-Albert, J., Yu, X. J., Beuzón, C. R., Blakey, A. N., Galyov, E. E., and Holden, D. W. (2002)
668 Complementary activities of SseJ and SifA regulate dynamics of the Salmonella typhimurium
669 vacuolar membrane. *Mol. Microbiol.* **44**, 645-661
670 55. Roy, C. R. (2012) Vacuolar pathogens value membrane integrity. *Proc. Natl. Acad. Sci. U. S. A.*
671 **109**, 3197-3198
672 56. Miller, M. B., and Bassler, B. L. (2001) Quorum sensing in bacteria. *Annu. Rev. Microbiol.* **55**, 165-
673 199
674 57. Edelstein, P. H. (1981) Improved semiselective medium for isolation of Legionella pneumophila
675 from contaminated clinical and environmental specimens. *J. Clin. Microbiol.* **14**, 298-303
676 58. Bertani, G. (1951) Studies on lysogenesis. I. The mode of phage liberation by lysogenic
677 Escherichia coli. *J. Bacteriol.* **62**, 293-300
678 59. Bingel-Erlenmeyer, R., Olieric, V., Grimshaw, J. P. A., Gabadinho, J., Wang, X., Ebner, S. G.,
679 Isenegger, A., Schneider, R., Schneider, J., Glettig, W., Pradervand, C., Panepucci, E. H., Tomizaki,
680 T., Wang, M., and Schulze-Briese, C. (2011) SLS Crystallization Platform at Beamline X06DA—A
681 Fully Automated Pipeline Enabling in Situ X-ray Diffraction Screening. *Crystal Growth & Design*
682 **11**, 916-923
683 60. Vonrhein, C., Flensburg, C., Keller, P., Sharff, A., Smart, O., Paciorek, W., Womack, T., and
684 Bricogne, G. (2011) Data processing and analysis with the autoPROC toolbox. *Acta Crystallogr. D*
685 *Biol. Crystallogr.* **67**, 293-302
686 61. Pape, T., and Schneider, T. R. (2004) HKL2MAP: a graphical user interface for macromolecular
687 phasing with SHELX programs. *Journal of Applied Crystallography* **37**, 843-844
688 62. Terwilliger, T. C., Grosse-Kunstleve, R. W., Afonine, P. V., Moriarty, N. W., Zwart, P. H., Hung, L.-
689 W., Read, R. J., and Adams, P. D. (2008) Iterative model building, structure refinement and
690 density modification with the PHENIX AutoBuild wizard. *Acta Crystallographica Section D* **64**, 61-
691 69
692 63. Emsley, P., Lohkamp, B., Scott, W. G., and Cowtan, K. (2010) Features and development of Coot.
693 *Acta Crystallogr. D Biol. Crystallogr.* **66**, 486-501
694 64. Winn, M. D., Ballard, C. C., Cowtan, K. D., Dodson, E. J., Emsley, P., Evans, P. R., Keegan, R. M.,
695 Krissinel, E. B., Leslie, A. G., McCoy, A., McNicholas, S. J., Murshudov, G. N., Pannu, N. S.,
696 Potterton, E. A., Powell, H. R., Read, R. J., Vagin, A., and Wilson, K. S. (2011) Overview of the
697 CCP4 suite and current developments. *Acta Crystallogr. D Biol. Crystallogr.* **67**, 235-242
698 65. Joosten, R. P., Long, F., Murshudov, G. N., and Perrakis, A. (2014) The PDB_REDO server for
699 macromolecular structure model optimization. *IUCrJ* **1**, 213-220
700 66. Afonine, P. V., Grosse-Kunstleve, R. W., Echols, N., Headd, J. J., Moriarty, N. W., Mustyakimov,
701 M., Terwilliger, T. C., Urzhumtsev, A., Zwart, P. H., and Adams, P. D. (2012) Towards automated
702 crystallographic structure refinement with phenix.refine. *Acta Crystallogr. D Biol. Crystallogr.* **68**,
703 352-367
704 67. Burkhardt, A. (2016) Status of the crystallography beamlines at PETRA III. *Eur. Phys. J. Plus* **131**
705 68. Mirdita, M., Schutze, K., Moriwaki, Y., Heo, L., Ovchinnikov, S., and Steinegger, M. (2022)
706 ColabFold: making protein folding accessible to all. *Nat Methods* **19**, 679-682
707 69. Flieger, A., Gongab, S., Faigle, M., Mayer, H. A., Kehrer, U., Mussotter, J., Bartmann, P., and
708 Neumeister, B. (2000) Phospholipase A secreted by Legionella pneumophila destroys alveolar
709 surfactant phospholipids. *FEMS Microbiol. Lett.* **188**, 129-133

710 70. Schromm, A. B., Brandenburg, K., Rietschel, E. T., Flad, H. D., Carroll, S. F., and Seydel, U. (1996)
711 Lipopolysaccharide-binding protein mediates CD14-independent intercalation of
712 lipopolysaccharide into phospholipid membranes. *FEBS Lett.* **399**, 267-271
713 71. Schrödinger, LLC. (2020) The PyMOL Molecular Graphics System, Version 2.4.
714 72. Jepras, R., Fitzgeorge, R., and Baskerville, A. (1985) A comparison of virulence of two strains of
715 Legionella pneumophila based on experimental aerosol infection of guinea-pigs. *Epidemiol.*
716 *Infect.* **95**, 29-38
717

718

719

720 **Abbreviations:**

721	CTD	C-terminal domain
722	ePC	L-α-phosphatidylcholine (chicken egg)
723	ecPE	L-α-phosphatidylethanolamine (*E. coli*)
724	FFA	free fatty acids
725	FRET	Förster-Resonance-Energy-Transfer
726	GCAT	glycerophospholipid:cholesterol acyltransferase
727	LCV	*Legionella*-containing vacuole
728		
729	LPLA	lysophospholipase A
730	NBD-PE	*N*-(7-nitrobenz-2-oxa-1,3-diazol-4-yl)-1,2-dihexadecanoyl-*sn*-
731		glycero-3-phosphoethanolamine
732	MW	molecular weight
733	PEG	polyethylene glycol
734	PLA/PLB/PLC/PLD	phospholipase A/B/C/D
735	Rho-DHPE	Lissamine™ Rhodamine B 1,2-dihexadecanoyl-*sn*-
736		glycero-3-phosphoethanolamine
737	SAD	single anomalous dispersion
738	SEC	size exclusion chromatography
739	SP	signal peptide
740	T2SS/T4SS	type II/IV secretion system
741	8:0 LPC	1-monooctanoyllysophosphatidylcholine
742	12:0 LPC	1-monolauroyllysophosphatidylcholine
743	14:0 LPC	1-monotetradecanoyllysophosphatidylcholine
744	16:0 LPC	1-monopalmitoyllysophosphatidylcholine
745	18:0 LPC	1-monostearoyllysophosphatidylcholine
746	20:0 LPC	1-monoarachidoyllysophosphatidylcholine
747	22:0 LPC	1-monobehenoyllysophosphatidylcholine
748		

749

750 **Tables**

751

752 **Table 1: Important protein characteristics** of *L. pneumophila* Corby GDSL enzymes PlaA, PlaC, and PlaD
753 Data are derived from this study and (26,27).NCBI Pprotein database (PlaA: WP_011947186.1; PlaC:
754 WP_011947718.1; PlaD: WP_011947511.1).

Protein characteristic	PlaA (lpc1811)	PlaC (lpc3121)	PlaD (lpc0558)
NCBI protein database	WP_011947186.1	WP_011947718.1	WP_011947511.1
Size / SP [amino acids]	309 / 18	433 / 24	519 / no SP predicted
MW [kDa]	34.4	49.7	59.6
MW w/o SP [kDa]	32.8	46.9	no signal peptide
MW w/o SP [kDa], processed	27.8	36.1	not applicable
Preferred ProA cleavage site	E266/L267	Potential sites: **Q366/Y367**, Y363/V364, Q372/Y373	Not applicable
Catalytic triad	S30, D279, H282	S37, D398, H401	S17, D341, H344
Central β-sheet	5 parallel	5 parallel	5 parallel + 1 antiparallel
additional helices in α/β-hydrolase fold	No	Yes (P57-G120 and D166-P193)	No
Lid / disulfide loop	yes (C243-C272)	yes (C343-C388)	no lid and no disulfide loop
Additional C-terminal domain	No	No	Yes (K400-T516)

755

756

757 **Table 2:** X-ray data collection and refinement statistics.
758

Structure PDB-ID:	PlaA iodide SAD 8A24	PlaA PEG complex 8A25	PlaA palmitate complex 8A26
Data collection[a]			
Beamline	SLS X06DA (PXIII; 2018/02/22)	SLS X06DA (PXIII; 2018/02/22)	PetraIII P11 (2018/05/29)
Wavelength (Å)	1.7712	1.3778	1.00
Space group	$P3_121$	$P3_121$	$P3_121$
Cell dimensions			
a, *b*, *c* (Å)	81.85, 81.85, 68.21	82.24, 82.24, 68.45	82.92, 82.92, 68.64
α, β, γ (°)	90, 90, 120	90, 90, 120	90, 90, 120
Resolution (Å)[b]	70.89 – 2.36 (2.41 – 2.36)	49.35 – 1.73 (1.76 – 1.73)	49.62 – 1.45 (1.48 – 1.45)
R_{merge} (%)[b]	18.9 (196.2)	6.4 (140.5)	6.3 (160.0)
R_{pim} (%)[b]	3.1 (32.1)	1.5 (32.3)	1.1 (29.6)
$I/\sigma(I)$[b]	21.4 (2.3)	28.5 (2.2)	33.6 (2.3)
Completeness (%)[b]	100.0 (100.0)	96.0 (100)	100.0 (100.0)
Redundancy[b]	38.4 (37.5) anomalous: 20.4 (19.5)	19.2 (19.8)	32.8 (29.8)
$CC_{1/2}$ (%)[b]	99.9 (83.9)	100 (74.4)	100 (82.3)
Refinement			
Resolution (Å)[b]	70.89 - 2.36 (2.45 - 2.36)	49.35 – 1.73 (1.79 – 1.73)	49.62 – 1.45 (1.50 – 1.45)
No. reflections[b]	11124 (1079)	27072 (2801)	48590 (4808)
R_{work} (%)[b]	22.81 (27.67)	15.96 (23.84)	15.55 (25.83)
R_{free} (%)[b]	27.91 (28.90)	18.54 (28.75)	17.74 (26.92)
No. atoms			
Protein	2206	2297	2319
Ligand/ion	13	59	115
Water	62	168	225
B-factors (Å^2)			
Protein	54	35	25
Ligand/ion	90	51	46
Water	53	39	37
R.m.s deviations			
Bond lengths (Å)	0.002	0.005	0.006
Bond angles (º)	0.44	0.800	0.930
Ramachandran			
Favored	94.6	97.21	97.19
Allowed	5.04	2.79	2.81
Outliers	0.36	0.00	0.00

759 [a]Values for the highest resolution shell are shown in parentheses.
760 [a]Data were indexed, integrated, scaled and merged with autoproc. The statistics reported here result
761 from isotropic treatment, using I/σ(I) > 2.0 as a high resolution cut-off.
762
763

764

765 **Table 3:** Overview of strains used in this study.

766 * -(SP): constructs cloned without sequence coding for the predicted signal peptide (aa 1-18), strain was
767 used for PlaA expression and purification for crystallization, X-ray diffraction, and structure
768 determination.

Organism	Mutation/Plasmid	Tag	Selection marker	Reference
L. pn. Corby	Wild type	-	-	(72)
E. coli BL21 (pCL119)	pGP172 plaA$_{Corby}$ (-SP)*	N-term. Strep-tag	Amp^R	(27)
E. coli BL21 (pCL121)	pGP172 plaA$_{Corby}$ S30N (-SP)	N-term. Strep-tag	Amp^R	(27)
E. coli BL21 (pCL126)	pGP172 plaA$_{Corby}$ ΔAA248-67(-SP)	N-term. Strep-tag	Amp^R	(27)
E. coli BL21 (pCL127)	pGP172 plaA$_{Corby}$ S30N ΔAA248-67 (-SP)	N-term. Strep-tag	Amp^R	(27)
E. coli BL21 (pMH41)	pGP172 plaA$_{Corby}$ E266N L267N (-SP)	N-term. Strep-tag	Amp^R	(27)
E. coli BL21 (pMH42)	pGP172 plaA$_{Corby}$ S30N E266N L267N (-SP)	N-term. Strep-tag	Amp^R	This study
E. coli BL21 (pCL15)	pet28a(+) proA$_{Corby}$	N-term. Strep-tag	Km^R	(26)
E. coli BL21 (pUS8)	pGP172 plaA$_{Corby}$ P283L (-SP)	N-term. Strep-tag	Amp^R	This study
E. coli BL21 (pUS9)	pGP172 plaA$_{Corby}$ T220L (-SP)	N-term. Strep-tag	Amp^R	This study

769

770

771

772

773

774 **Figure Legends**

775

776 **Figure 1: Crystal structure of *Legionella pneumophila* PlaA in complex with palmitic acid shows that**
777 **the disulfide loop covers the catalytic triade.**

778 (A) Schematic overview of *L. pneumophila* PlaA, PlaC, and PlaD showing the location of the SP, the
779 catalytic triade, the disulfide loop (only found in PlaA and PlaC) and molecular weights of unprocessed
780 proteins Adapted from (27). (*B*) cartoon representation of PlaA structure, colored from blue at the N-
781 terminus to red at the C-terminus. Important residues of the active site (catalytic triad: S30, D279, H282)
782 and the limiting residues (C243, C272) of the disulfide loop (orange) are shown as sticks (carbon: yellow,
783 oxygen: red, nitrogen: blue, sulfur: gold), together with the product palmitic acid (carbon: black). The
784 ProA cleavage site resides within the disulfide loop. (*C*) cross-eyed stereoplot of the PlaA substrate
785 binding site. Palmitic acid is shown in black, the ligand binding cavity is shown in grey. Residues that
786 contribute to the binding site are shown as sticks (carbon: green). (*D*) surface representation of PlaA.
787 The protein is in the same orientation as in *B*. Note that the disulfide loop shown in yellow shields the
788 active site fully. Abbreviations: SP – predicted signal peptide, AA – amino acid(s), S-S bridge – predicted
789 disulfide bond

790

791 **Figure 2: Crystal structures of selected proteins related to *L. pneumophila* PlaA according to analysis**
792 **with DALI** (39)**.**

793 Ribbon representations with residues of the catalytic triad in the active site are shown as sticks on the
794 left; top views of the molecular surface are shown on the right. Residues of the disulfide loops are
795 plotted in yellow. Oxygen and nitrogen atoms of the catalytic triad are shown in red and blue,
796 respectively. (*A*) Crystal structure of *L. pneumophila* PlaA in complex with palmitic acid. (*B*) *P. aeruginosa*
797 ChoE is an acetylcholinesterase (PDB entry 1uqv) (40). (*C*) *V. vulnificus* PlpA is a type II-secreted
798 phospholipase A2 that utilizes a chloride ion (green sphere) instead of aspartate in its catalytic triad (PDB
799 entry 6jkz) (41). (*D*) EstA is an autotransported esterase displayed on the outer membrane of *P.*
800 *aeruginosa*. The autotransporter domain is shown in darker colors (PDB entry 3kvn) (42). Note that ChoE,
801 PlpA and EstA have significantly shorter disulfide loops than PlaA, which makes their active sites solvent-
802 accessible.

803

804 **Figure 3: Deletion of the disulfide loop in PlaA increases membrane interaction.**

805 Protein-membrane interaction of PlaA S30N and disulfide loop deletion mutant PlaA S30N ΔAA248-267
806 was monitored by FRET spectroscopy. An increase of the intensity ratio $I_{donor}/I_{acceptor}$ corresponds to a
807 reduced FRET efficiency and indicates insertion of proteins into the ePC:ecPE (1:1) liposomes.
808 Experiments were performed in 40 mM Tris, 150 mM NaCl, pH 7.5, at 37 °C. Donor and acceptor
809 intensities of the liposomes were both adjusted to 300,000 cps. PlaA variant concentrations of 1, 5, 10,
810 30, 50, and 100 µg/ml were titrated into the liposome solution and the respective values were
811 determined 5 min after injection when a steady state was reached. Experiments were repeated four
812 times and the data are shown as means and standard deviation (n=4).

813

814 **Figure 4: PlaA prefers 16:0 lysophospholipids for hydrolysis and a P283L mutation in the substrate**
815 **binding pocket changes substrate preference to shorter fatty acids**

816 (*A, B*) -LPLA activities of PlaA and PlaA variants were determined via quantification of free fatty acids
817 (FFA) after incubation for 1 h with the indicated lipids at 37 °C. (A) 200ng recombinant protein of PlaA
818 and its catalytic inactive mutant PlaA S30N (left side) or a disulfide loop truncation mutant PlaA
819 ΔΔAA248-67 and its catalytic inactive mutant PlaA S30N ΔΔAA248-67 (right side) were used for the
820 assay. (B) Cell lysates of strains expressing PlaA and PlaA mutants in the substrate binding site, such as
821 PlaA P283L or PlaA T220L, were used and diluted 1:2. Location of the mutated residue P283L is shown in
822 Fig. 1C and mutated residues P283L and T220L in Fig. S2. Data are shown as means and standard
823 deviation (n=3) and are representative for at least two additional experiments.

824

825 **Figure 5: Processing of PlaA occurs from mid-logarithmic growth and PlaA activation by ProA is not**
826 **inhibited by mutation of E266/L267 highlighting ProA's broad cleavage site acceptance**

827 *(A)* The growth of *L. pneumophila* wild type in broth was monitored over a period of 7 h and samples of
828 culture supernatants were analyzed for the presence, processing status of PlaA *(B)*, and presence of
829 ProA *(C)* by Western blotting with PlaA- and ProA-directed antibodies, respectively. Molecular weight
830 standards are shown on the left of the Western blots. The data are representative for one additional
831 experiment. (*D*) LPLA activities of recombinant PlaA (25 ng), a PlaA variant mutated in the preferred
832 cleavage site E266N L267N and catalytic inactive S30N mutants of both were determined via
833 quantification of free fatty acids (FFA) after incubation for 3 h with 16:0 LPC at 37 °C. Reactions were
834 performed without or with addition of 3.5 mU ProA as indicated. (*E*) Western Blots using PlaA-directed
835 antibodies after incubation of PlaA and a mutant in the preferred cleavage site E266N L267N without

836 and with addition of ProA for 10 min and 1 h. ProA-derived processing occurred for both types of PlaA.
837 (*D*) Data are shown as mean and standard deviation (n=3) and (D and E) are representative for three
838 additional experiments.
839
840 **Figure 6: AlphaFold** (46) **predicted structures of the three *L. pneumophila* GDSL phospholipases PlaA,**
841 **PlaC, and PlaD.**
842 Representations, orientations and color schemes are similar to Fig. 2. (*A*) AlphaFold model of PlaA from
843 *L. pneumophila* strain Corby (NCBI Protein database entry WP_011947186.1). Note the correct prediction
844 of the position of the disulfide loop with respect to the experimental structure (compare to Fig. 2A and
845 Fig. S2A-C), leading to a shielded active site. (*B*) AlphaFold model of PlaC from *L. pneumophila* strain
846 Corby (NCBI Protein database entry WP_011947718.1). The predicted position of the disulfide loop leads
847 to a similar shielding as in PlaA. (*C*) AlphaFold model of PlaD from *L. pneumophila* strain Corby (NCBI
848 Protein database entry WP_011947511.1). PlaD does not contain a disulfide loop; residues structurally
849 corresponding to the disulfide loop of PlaA are shown in light blue. The predicted additional C-terminal
850 domain of unknown function of PlaD is shown in light green. Note that the active site of PlaD is predicted
851 to be solvent-exposed, however, the C-terminal domain may position itself to block access to the active
852 center.
853
854
855

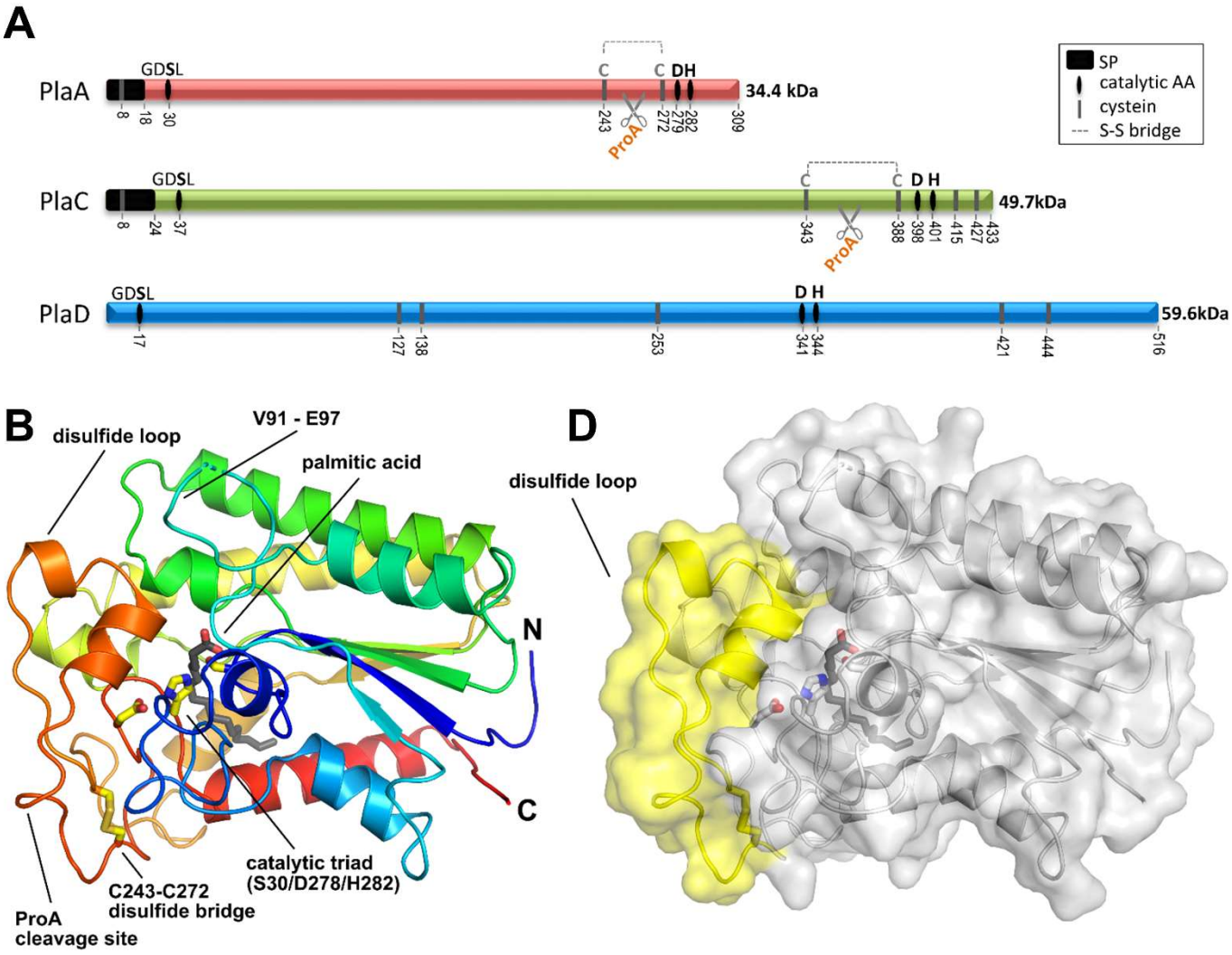

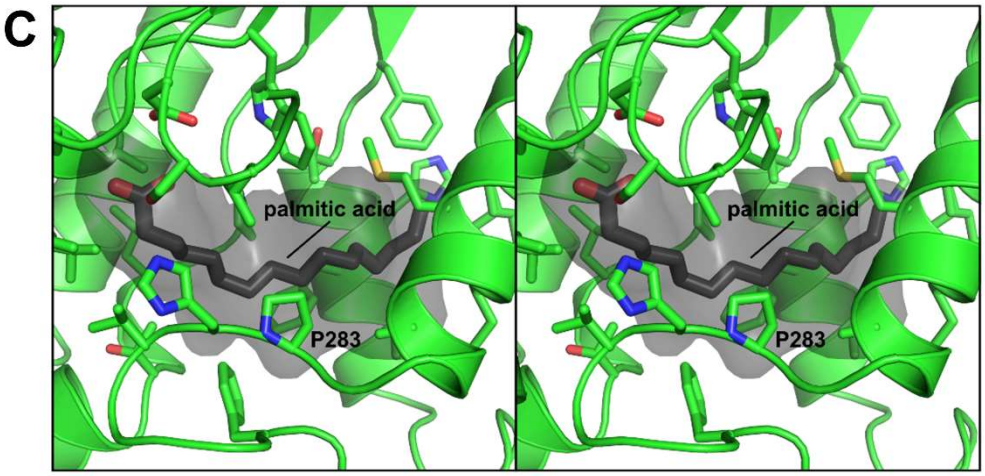

Hiller, Diwo *et al*. Fig. 1

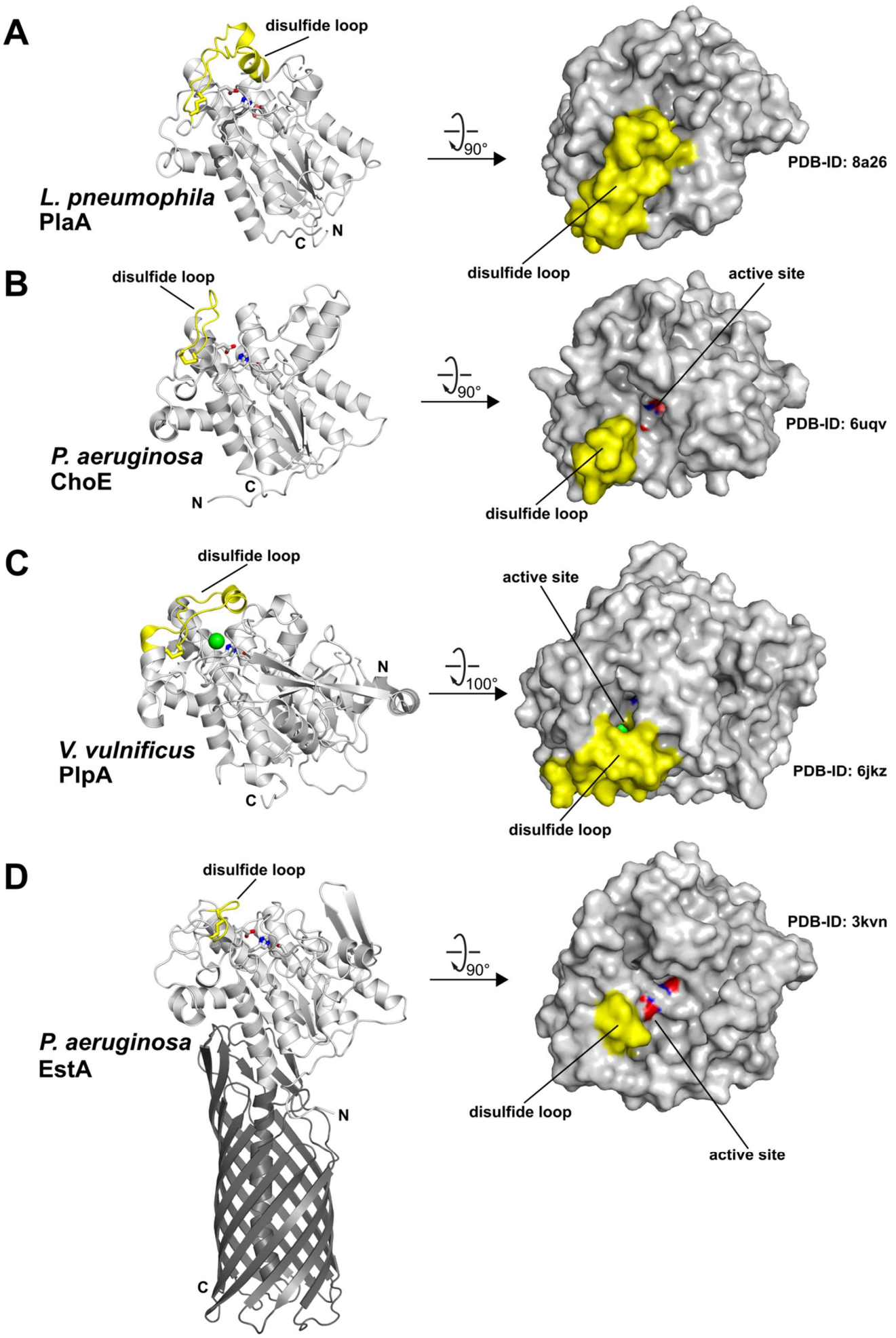

Hiller, Diwo *et al*. Fig. 2

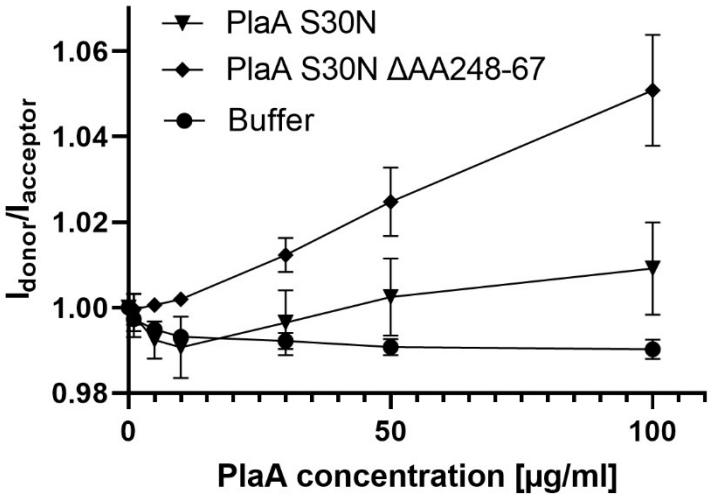

Hiller, Diwo *et al*. Fig. 3

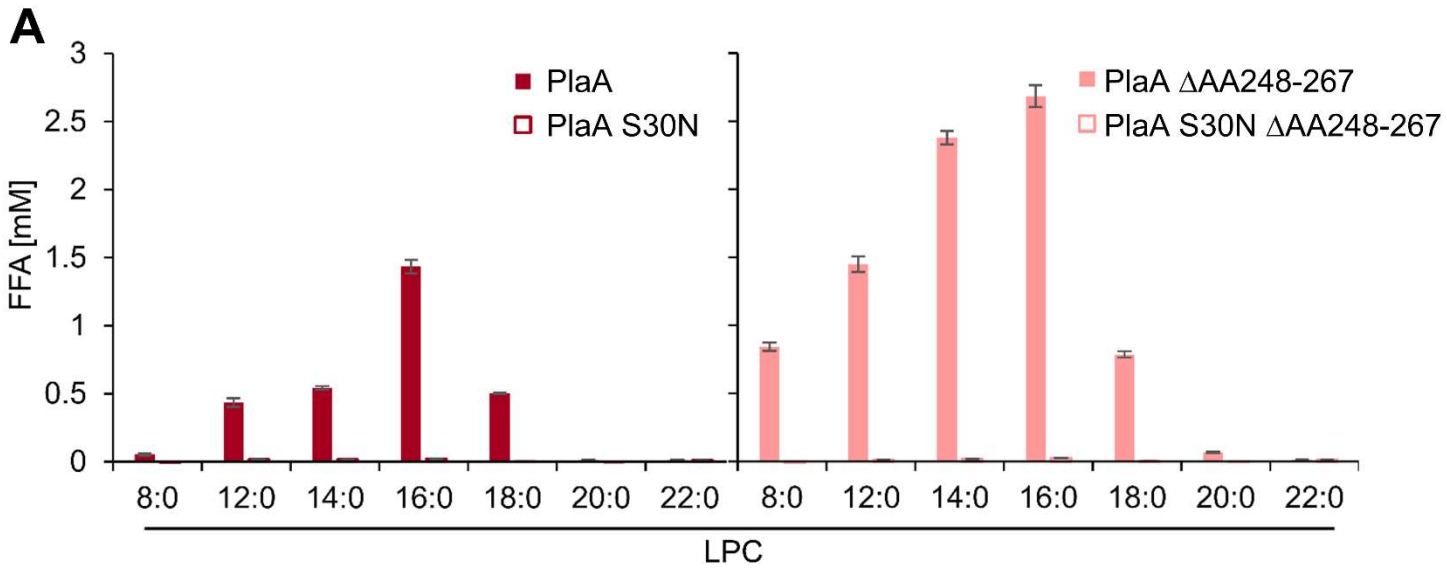

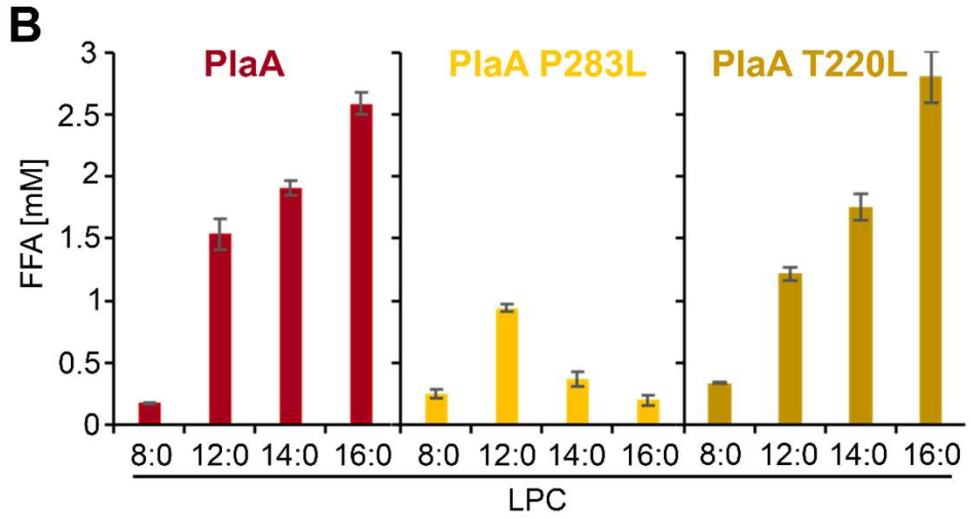

Hiller, Diwo *et al*. Fig. 4

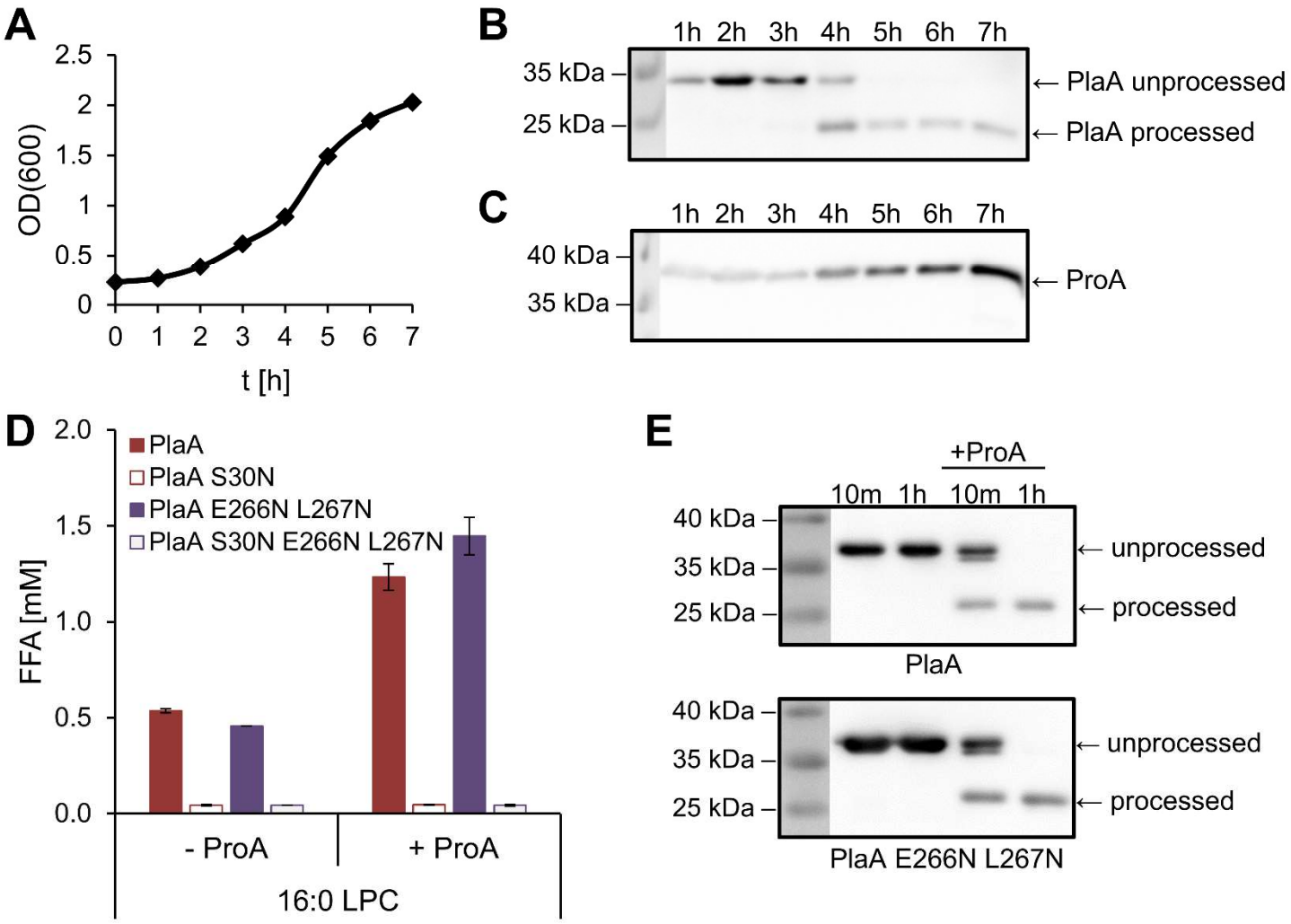

Hiller, Diwo *et al*. Fig. 5

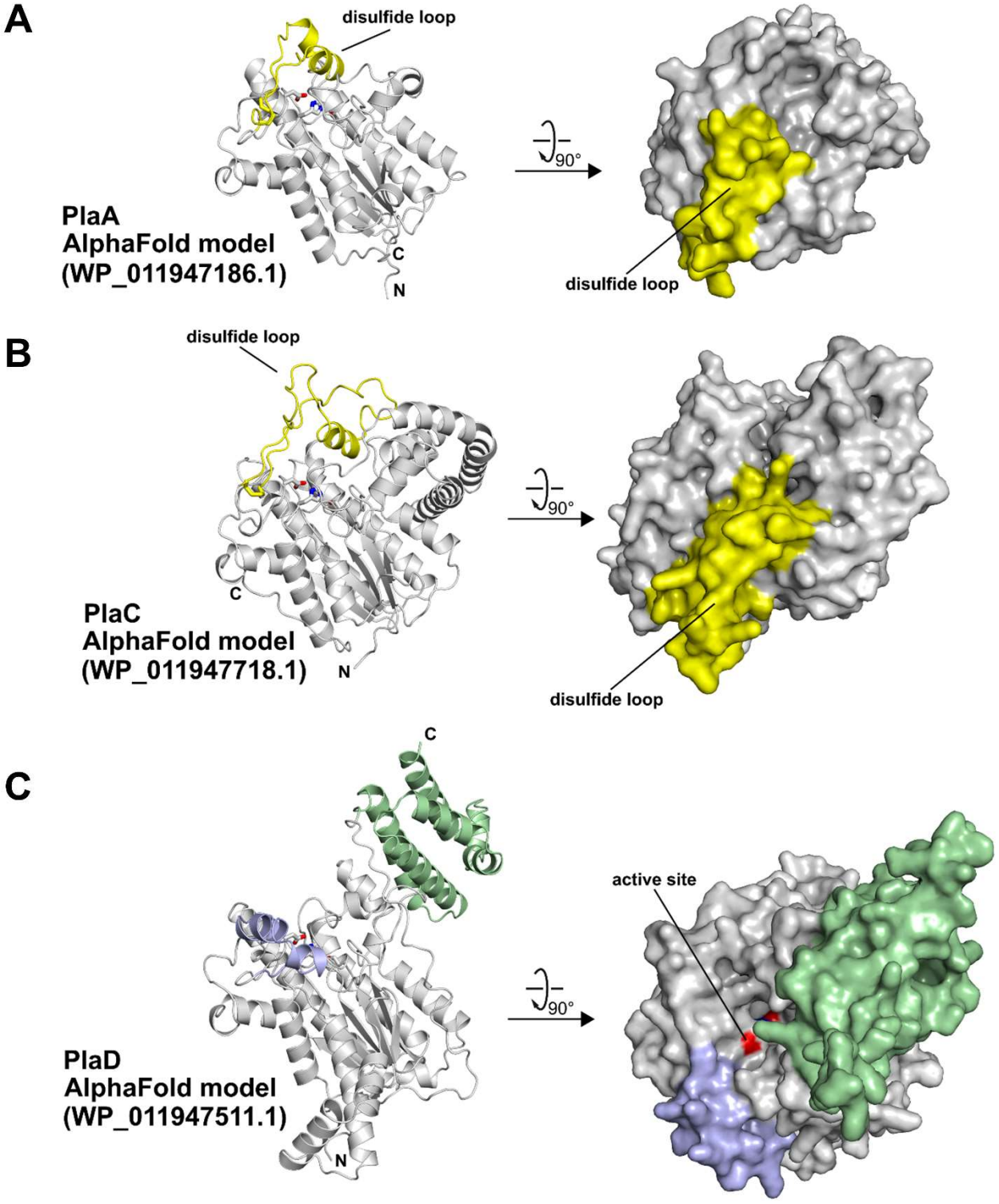

Hiller, Diwo *et al*. Fig. 6